ISSN 1674-1056
http://cpb.iphy.ac.cn
http://iopscience.iop.org/cpb
中国物理 B
Chinese Physics
中国物理
Chinese Physics B

Effect of thermally induced birefringence on high power picosecond azimuthal polarization Nd:YAG laser system

Hongpan Peng(彭红攀), Ce Yang(杨策), Shang Lu(卢尚), Ning Ma(马宁), Meng Chen(陈檬)

Citation: Chin. Phys. B . 2019, 28(2): 024205. **doi:** 10.1088/1674-1056/28/2/024205
Journal homepage: http://cpb.iphy.ac.cn; http://iopscience.iop.org/cpb

What follows is a list of articles you may be interested in

Analysis of CV mode selected resonator based on vectorial eigenvector method

You-You Hu(胡友友), Jian-Tai Dou(窦健泰), Bo-Wei Luo(罗博伟), Chang-Yu He(贺昌玉)

Chin. Phys. B . 2019, 28(2): 024210. **doi:** 10.1088/1674-1056/28/2/024210

Coupled resonator-induced transparency on a three-ring resonator

Xinquan Jiao(焦新泉), Haobo Yu(于皓博), Miao Yu(于淼), Chenyang Xue(薛晨阳), Yongfeng Ren(任勇峰)

Chin. Phys. B . 2018, 27(7): 074212. **doi:** 10.1088/1674-1056/27/7/074212

Birefringence via Doppler broadening and prevention of information hacking

Humayun Khan, Muhammad Haneef, Bakhtawar

Chin. Phys. B . 2018, 27(1): 014201. **doi:** 10.1088/1674-1056/27/1/014201

Coupled-resonator-induced transparency in two microspheres as the element of angular velocity sensing

Kun Qian(钱坤), Jun Tang(唐军), Hao Guo(郭浩), Wei Zhang(张伟), Jian-Hua Liu(刘建华), Jun Liu(刘俊), Chen-Yang Xue(薛晨阳), Wen-Dong Zhang(张文栋)

Chin. Phys. B . 2016, 25(11): 114209. **doi:** 10.1088/1674-1056/25/11/114209

Coupled thermal-optic effects and electrical modulation mechanism of birefringence crystal with Gaussian laser incidence

Zhou Ji, He Zhi-Hong, Ma Yu, Dong Shi-Kui

Chin. Phys. B . 2015, 24(9): 094203. **doi:** 10.1088/1674-1056/24/9/094203

Effect of thermally induced birefringence on high power picosecond azimuthal polarization Nd:YAG laser system*

Hongpan Peng(彭红攀), Ce Yang(杨策), Shang Lu(卢尚), Ning Ma(马宁), and Meng Chen(陈檬)†

Laser Engineering Research Institute, Beijing University of Technology, Beijing 100124, *China*

(Received 13 November 2018; revised manuscript received 4 December 2018; published online 10 January 2019)

Pulse-burst 1064-nm picosecond azimuthal polarization beam amplification up to an average power of 16.32 W using side-pumped Nd: YAG amplifiers has been demonstrated. The maximum envelop energy as much as 16.32 mJ, corresponding to a power amplification factor of 299.5%. A simple criterion was defined to help estimate the amount of depolarization in Nd:YAG amplifier stages. The degree of depolarization of the beam was 7.1% and the beam quality was measured to be $M^2 = 3.69$. The reason for the azimuthal polarization depolarization and beam quality degradation were explained theoretically and experimentally during the amplification process.

Keywords: azimuthal polarization, thermally induced birefringence, Nd:YAG amplifiers, picosecond laser

PACS: 42.25.Lc, 42.60.Da, 42.65.Re, 29.25.Lg **DOI:** 10.1088/1674-1056/28/2/024205

1. Introduction

In recent years, following the development of lasers in industrial applications, high power cylindrical vector polarization lasers have become important for applications such as industrial cutting and drilling. Compared with a beam with linear or circularly polarized laser radiation, a beam with azimuthal or radial polarization is more efficient in producing holes of the same diameter and depth for steel.[1] Azimuthal polarization has been recommended for the generation of high aspect ratios in thick sheets or for very small diameters.[2] A continuous radially polarized laser with an average power of 2.1 kW and $M^2 < 10$ was obtained using Nd:YAG rod amplifiers.[3] An energy as high as 772 mJ at 10 Hz with a 10-ns pulse using flash-lamp-pumped Nd:YAG amplifiers was obtained recently.[4] Radial polarization amplification has been reported but there have been no studies of picosecond pulse burst azimuthally polarized beam amplification.

The aim of this work is to amplify the picosecond pulse-bursts of an azimuthally polarized beam by means of a transversally pumped Nd:YAG crystal. The amplification method is simple, power scalable, reliable and robust. In addition, the important property of azimuthal polarization radiation allows us to bypass thermal birefringence induced aberrations, which significantly affect linearly polarized, circularly polarized beams.[5] However, when increasing the operating power of a solid-state laser, the thermal load increases proportionally, which enhances the thermally induced birefringence.[6,7] This causes high losses for good beam quality. This work theoretically explains the depolarization effect of thermally induced birefringence caused by the non-uniformity of the transversally pump and also reflects the beam quality deteriorates from three aspects: intensity distribution, the beam quality M^2 factor, and azimuthal polarization purity.

In general, an azimuthally polarized beam has been obtained in a laser cavity or extra-cavity.[8–12] In the experiment, azimuthally polarized radiation was converted via an extra-cavity polarization converter. Interestingly, the seed beam used in this work is a pulse burst picosecond azimuthally polarized beam. Ultra-short pulse burst have a variety of applications in the field of material processing.[13] Therefore, the beam amplified in this work provides a new source reference for material processing.

In this work, an amplification of picosecond pulse burst azimuthally polarized beam in two transversally pumped Nd:YAG amplifier stages is reported. This amplifier system yielded an average power of 16.32 W at 1064 nm, corresponding to an amplification factor of 299.5%. The pulse envelope energy, consisting of four pulses with equal amplitude and 1-ns pulse spacing, was 16.32 mJ, which is the highest pulse energy achieved for picosecond azimuthal polarization. To the best of our knowledge, this is the first study of picosecond pulse burst azimuthally polarized beam amplification in a bulk solid-state amplifier, and it attained the highest energy yet at 1 kHz and a 250-ps pulse width. The degree of depolarization of output beam was measured to be 7.1% and the beam quality was measured to be $M^2 = 3.69$. The second part will analyze the cause of the depolarization of azimuthal polarization caused by thermally induced birefringence.

*Project supported by the National Natural Science Foundation of China (Grant No. U1631240), the Education Commission Program of Beijing, and Beijing Natural Science Foundation (Grant No. KZ201510005001).

†Corresponding author. E-mail: chenmeng@bjut.edu.cn

© 2019 Chinese Physical Society and IOP Publishing Ltd

2. Theory

In this paper, the theoretical analysis of the depolarization in the process of azimuthal polarization amplification was carried out, and the depolarization effect caused by the transverse and longitudinal shear stress was numerically simulated. The simulation model is shown in Fig. 1. The three rows of LD are distributed around the crystal rod with an interval of 120°. The central pump region of the crystal rod is 30 mm, and the non-pump region is 16.5 mm at both ends. This laser rod has a diameter of 4 mm and a length of 63 mm. Since a large amount of heat is generated inside the crystal rod during the pumping process, water circulation is required around the crystal rod to carry the heat away. The water temperature was set to 23°.

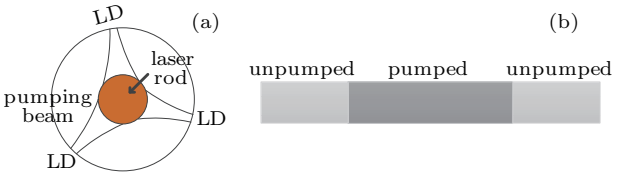


Fig. 1. The crystal rod pumping model. (a) Cross-section pump distribution of the rod, (b) Longitudinal pump distribution of the rod.

2.1. Influence of shear stress on the depolarization of azimuthal polarization beam in cross section

In this work, an Nd:YAG rod was investigated as a magnifying crystal, with its axis in the direction [111]. The thermally induced birefringence of the non-radial symmetric stress was determined in a coordinate system that coincides with the cylindrical axis of the rod. The strain tensor terms, produced by the stress terms (σ_{kl}) in the rod, are given as follows:[14]

$$\begin{aligned}
\varepsilon_r &= \frac{1}{E}\left[\sigma_r - \nu\left(\sigma_\varphi + \sigma_z\right)\right],\\
\varepsilon_\varphi &= \frac{1}{E}\left[\sigma_\varphi - \nu\left(\sigma_r + \sigma_z\right)\right],\\
\varepsilon_z &= \frac{1}{E}\left[\sigma_z - \nu\left(\sigma_\varphi + \sigma_r\right)\right],\\
\varepsilon_{r\varphi} &= \frac{1}{E(1+\nu)}\sigma_{r\varphi},
\end{aligned} \tag{1}$$

where ν is the Poisson ratio and E is Young's modulus. Previously, when the thermotropic refractive index change was studied, the analysis of the thermally induced stress in YAG assumes that the YAG crystal is elastic isotropic,[1] in which case the shear stress and strain term vanished, and a radial symmetric stress birefringence effect was obtained. However, this is just an approximation — in an actual non-uniform pumping system, it is responsible for the depolarization. In a non-uniformly pumped laser rod, the relative dielectric impermeable component ΔB_{ij} expression, including shear strain, can be obtained for a plane perpendicular to the beam propagation direction (z direction) in radial coordinates[14]

$$\left(B^0 + \Delta B_{rr}\right) r^2 + \left(B^0 + \Delta B_{\varphi\varphi}\right) \varphi^2 + 2\Delta B_{r\varphi} r\varphi = 1, \tag{2}$$

$$\begin{aligned}
\Delta B_{rr} &= P_{11}\varepsilon_{rr} + P_{12}\varepsilon_{\varphi\varphi},\\
\Delta B_{\varphi\varphi} &= P_{12}\varepsilon_{rr} + P_{11}\varepsilon_{\varphi\varphi},\\
\Delta B_{r\varphi} &= P_{66}\varepsilon_{r\varphi},
\end{aligned} \tag{3}$$

$$\begin{aligned}
P_{11} &= \frac{1}{2}p_{11} + \frac{1}{2}p_{12} + p_{44},\\
P_{12} &= \frac{1}{6}p_{11} + \frac{5}{6}p_{12} - \frac{1}{3}p_{44},\\
P_{66} &= \frac{1}{6}p_{11} - \frac{1}{6}p_{12} + \frac{2}{3}p_{44},
\end{aligned} \tag{4}$$

$$\Delta n_{ij} = \frac{1}{2}n_0^3 \Delta B_{ij}, \tag{5}$$

where, p_{11}, p_{12}, and p_{44} are the photoelastic coefficients of the crystal.

In this experiment, $\Delta n_{r\varphi}$ is an aberration and is responsible for the destruction of birefringence radial symmetry. In the Cartesian coordinate system, the beam is transmitted along the z axis (the direction of the crystal axis [111]).

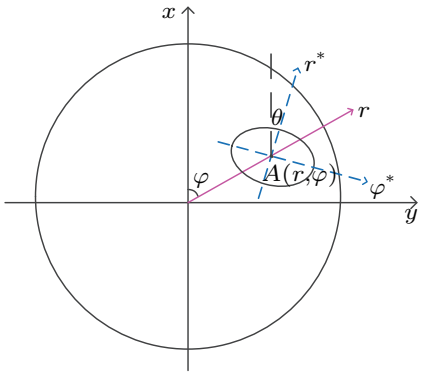


Fig. 2. Relationship between refractive index ellipse and crystal plane coordinates.

We only consider the refractive index ellipsoid equation at any point A in the plane perpendicular to the z axis (as shown in Fig. 2)[15]

$$\left(B_0 + \Delta B_{xx}\right) x^2 + \left(B_0 + \Delta B_{yy}\right) y^2 + 2\Delta B_{xy} xy = 1. \tag{6}$$

The standard equation after normalizing Eq. (6) along the elliptical major axis is:

$$\left(B_0 + \Delta B_{x^*x^*}\right) x^{*2} + \left(B_0 + \Delta B_{y^*y^*}\right) y^{*2} = 1. \tag{7}$$

Comparing Eqs. (6) and (7) gives

$$\tan\left(2\theta\right) = \frac{2\Delta B_{xy}}{\Delta B_{xx} - \Delta B_{yy}}. \tag{8}$$

To research the effect of a non-uniformly pumped laser rod on an azimuthally polarized beam, a transformation matrix H is needed for coordinate transformation, which obeys

$$\begin{pmatrix} \Delta B_{xx} & \Delta B_{xy} \\ \Delta B_{xy} & \Delta B_{yy} \end{pmatrix} = H \begin{pmatrix} \Delta B_{rr} & \Delta B_{r\varphi} \\ \Delta B_{r\varphi} & \Delta B_{\varphi\varphi} \end{pmatrix} H^{-1}, \tag{9}$$

$$H = \begin{pmatrix} \cos\varphi & -\sin\varphi \\ \sin\varphi & \cos\varphi \end{pmatrix}. \tag{10}$$

From Eqs. (8), (9), and (10) one can obtain

$$\tan(2\theta) = \frac{(P_{11}-P_{12})(\varepsilon_{rr}-\varepsilon_{\varphi\varphi})\sin 2\varphi + 2P_{66}\varepsilon_{r\varphi}\cos 2\varphi}{(P_{11}-P_{12})(\varepsilon_{rr}-\varepsilon_{\varphi\varphi})\cos 2\varphi - 2P_{66}\varepsilon_{r\varphi}\sin 2\varphi}. \quad (11)$$

The more uniform the thermal effect of the pump laser on the crystal rod, the less shear strain is produced. When the shear strain is close to zero, it is known from Eq. (11) that θ and φ are equal, so that an azimuthally polarized beam passes through the crystal without depolarization. However, in actual side pump amplification systems (such as those used in this experiment), shear stress and strain are present. Thus, the eigen polarizations of the crystal, the radial and azimuthal polarizations, differ from the original result.[10] The difference in refractive index of the major axis caused by the thermally induced birefringence effect can be expressed as:

$$n_{x^*} - n_{y^*} = -\frac{n_0^3}{2}\sqrt{(\Delta B_{xx}-\Delta B_{yy})^2 + 4\Delta B_{xy}{}^2}. \quad (12)$$

By taking the corresponding values into the above equation, the stress birefringence distribution caused by the shear stress in the cross section can be obtained, as shown in Fig. 3.

It can be seen from Fig. 3 that the thermal stress birefringence effect in the central region is much smaller than the birefringence effect of the surrounding region, and the birefringence effect gradually increases with the increase of the radius. In addition, the thermal birefringence effect on the same radius, the value and the variation along the azimuthal direction are obvious with r increasing. This indicates that the presence of shear stress in the cross section results in a thermally induced birefringence effect, which caused the occurrence of depolarization.

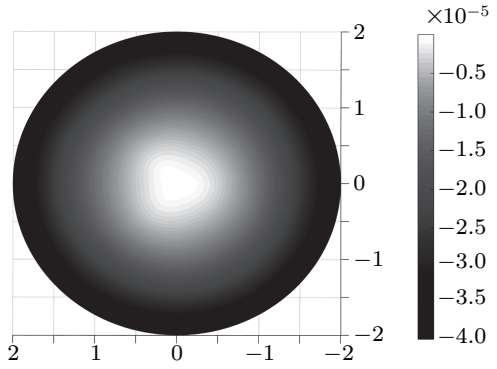


Fig. 3. Thermal stress birefringence distribution in cross section.

The optical path difference distribution of the entire surface can be obtained, which is derived from the thermal stress birefringence at each point. Its distribution is similar to stress birefringence. This shows that when the azimuthally polarized light passes through an amplification system with uneven temperature distribution, depolarization and beam quality degradation will occur.

2.2. The effect of longitudinal shear stress on the depolarization of azimuthal polarization beam

The x–z plane of the crystal rod was chosen as an example to analyze the effect of longitudinal shear stress on azimuthal polarization beam. The elliptic equation of the refractive index on this plane is:

$$(B_0+\Delta B_{xx})x^2 + (B_0+\Delta B_{zz})z^2 + 2\Delta B_{xz}xz = 1. \quad (13)$$

Convert Eq. (13) to the standard equation along the major axis of the refractive index ellipse:

$$(B_0+\Delta B_{x^*x^*})x^{*2} + (B_0+\Delta B_{z^*z^*})z^{*2} = 1. \quad (14)$$

Compare Eqs. (13) and (14) to get the formula:

$$\Delta B_{x^*x^*} = \frac{1}{2}(\Delta B_{xx}+\Delta B_{zz}) + \frac{1}{2}\sqrt{(\Delta B_{xx}-\Delta B_{zz})^2 + 4\Delta B_{xz}{}^2}, \quad (15)$$

$$\Delta B_{z^*z^*} = \frac{1}{2}(\Delta B_{xx}+\Delta B_{zz}) - \frac{1}{2}\sqrt{(\Delta B_{xx}-\Delta B_{zz})^2 + 4\Delta B_{xz}{}^2}. \quad (16)$$

Similar to the cross section, the stress birefringence in the plane is:

$$n_{x^*} - n_{z^*} = -\frac{n_0^3}{2}\sqrt{(\Delta B_{xx}-\Delta B_{zz})^2 + 4\Delta B_{xz}{}^2}. \quad (17)$$

The corresponding values were also introduced, and the stress birefringence distribution caused by shear stress in the x–z plane is shown in Fig. 4.

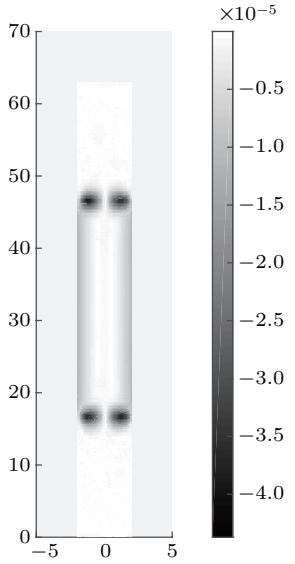


Fig. 4. Thermal stress birefringence distribution in longitudinal section (yellow is background in the figure).

As shown in Fig. 4, the thermal induced birefringence has the greatest influence at the junction of the pump region and the non-pump region, and the influence of other regions is small. Similarly, one can obtain the optical path difference of

the entire surface, which is derived from the value of the thermal stress birefringence at each point. This partial analysis demonstrates that there are some regions in the longitudinal direction that causes thermally induced birefringence, so the longitudinal direction is a non-negligible for the depolarization of azimuthally polarized beam.

These two parts have mainly studied the influence of stress birefringence on the depolarization performance of azimuthally polarized beams caused by heat distribution inhomogeneity. Therefore, this paper not only carried out the amplification experiment of the azimuthally polarized beam but also carried out the depolarization analysis of the amplified beam. In the subsequent laser amplification experiment, it is necessary to measure the depolarization of the obtained 16.32 W azimuthally polarized light, which is also the reason for measuring the degree of depolarization.

3. Experiments and results

A schematic diagram of experiment device is shown in Fig. 5. An all-solid-state pulse burst picosecond 1064-nm laser was used as the master laser at 1 kHz.[13] The pulse-burst were composed of four pulses with equal amplitude and a pulse spacing of 1 ns. The laser had an output average power of 7.27 W and pulse width of approximately 250 ps with a linear polarization beam. A spatially variant half-wave plate (S wave plate, Altechna) was used to convert the linearly polarized beam into an azimuthal polarization beam. The 5.45-W azimuthal polarization beam used as the seed beam was converted through the S-wave plate (double-sided plating with 1064-nm anti-reflection film, and a polarization conversion efficiency of 75%). A Faraday rotator and a half-wave-plate (HWP) were used to prevent any strong backward output from the amplifier from entering the master laser. The two amplifiers were designed to side-pump Nd:YAG rods (4-mm diameter by 63-mm length with a 30 mm pump length) using 12 horizontal diode arrays, based on three-rows, emitting at a wavelength of 808 nm. Up to 544-W average pump power output was obtained, corresponding to the pump pulse width of 200 μs and a frequency of 1 kHz. Before the seed beam entered the crystal amplifier, the beam expander was placed at a distance of 20 mm from the crystal plane to obtain better pattern matching. A negative lens was inserted at a 10-mm distance from the end of the first rod to prevent damage. Finally, the amplified laser was incident on a power meter or beam quality analyzer, which was used to measure the power or analyze the beam quality factor.

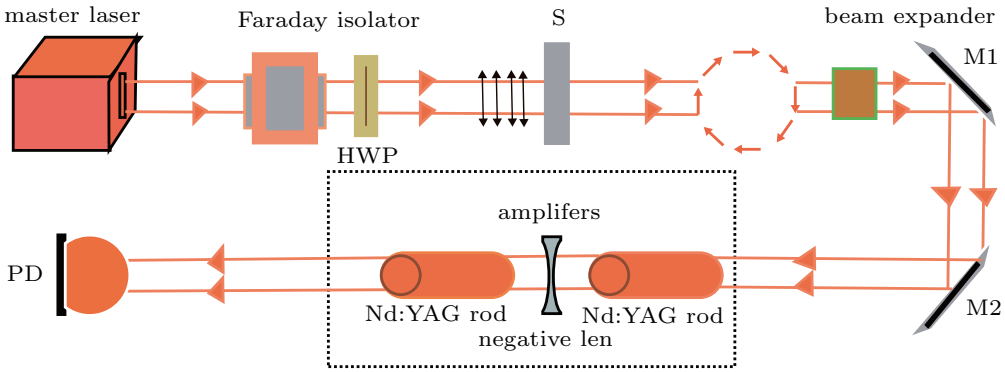


Fig. 5. Azimuthal polarization laser amplifier setup. S wave-plate: space variant polarization converter. M1 and M2: total reflective mirrors for 1064 nm. PD: photo detector.

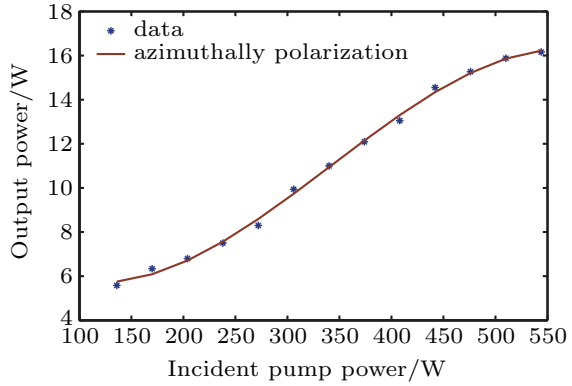


Fig. 6. Amplification output power as a function of incident pump power.

As shown in Fig. 6, a maximum amplification output average power of 16.32 W was obtained at a seed beam average power of 5.45 W, corresponded to a power amplification factor of 299.5%. The pulse envelope energy and the single pulse energy were 16.32 mJ and 4.08 mJ, respectively. This was the highest value that the azimuthally polarized output of the power amplifier had not yet obtained. Because of the characteristics of the gain module, it can be observed that the increment in output power gradually decreases as the pump power increases.

The amplified laser output and seed beam were sent through a convex lens with a focal length of 300 mm and sampled by the beam sampler, respectively. Images were observed in the focus using a charge-coupled device (CCD)-based beam profiler (Ophir, SP620U). Neutral density filters were installed

in front of the beam sampler to avoid damage to the CCD, which caused inconsistent colors in the captured image. Figure 7(a) shows the total intensity distribution of the seed beam. Obviously, it manifests a circular spatial profile with a dark center, which conforms to the intensity distribution of the azimuthally polarized beam. A linear polarizer was installed at Brewster's angle before the beam sampler to further confirm the polarization state of the seed beam. Figure 7(b) is the intensity distribution of the seed beam after passing through the linear polarizer and its intensity distribution was the upper and lower speckle. The beam (Fig. 7(c)), reflected by the polarizer, was distributed left and right. These results confirm that the seed beam converted by the S-wave plate was azimuthally polarized.

The amplified output intensity distribution at maximum pump is presented in Figs. 7(d)–7(f). Figure 7(d) is the total intensity distribution of the amplified beam. Figures 7(e) and 7(f) are the intensity distributions transmitted through the polarizer and reflected by the polarizer, respectively. The intensity and polarization distribution of the azimuthally polarized beam were substantially maintained during the amplification of the Nd:YAG amplifiers. However, the total intensity and polarization distribution of the amplified beam were not perfect compared with the seed beam. The non-radial symmetry differences of Figs. 7(a) and 7(d) are compared, which was contributed by the $\Delta n_{r\varphi}$ term. These were mainly responsible for the birefringence of uneven heat distribution, which were analyzed in the previous theoretical section.

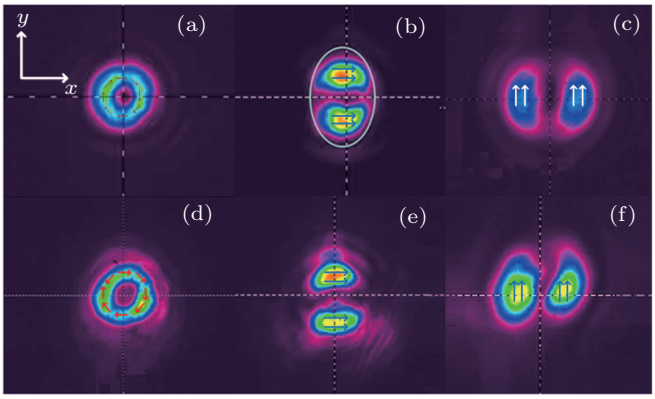


Fig. 7. Intensity distribution of the seed beam (top row), amplified output at maximum pumping power (bottom row). Panels (a) and (d) are total intensity distributions, panels (b) and (e) are intensity distributions after passing through the linear polarizer, panels (c) and (f) are intensity distributions reflected by the polarizer. These arrows indicate the direction of polarization.

To further investigate the thermal effects on the amplification of an azimuthally polarized beam, this work measured the degree of depolarization as a function of pumping power, as shown in Fig. 8. The beam transmitted through the polarizer at a Brewster's angle was horizontally polarized and reflected by the polarizer was vertically polarized. The power for a completely azimuthally polarized beam transmitted through the polarizer, and reflected by the polarizer should be equal. However, figure 8 shows that the degree of depolarization is gradually greater as the pump power increases. This shows that the polarization state of the amplified output was not completely axisymmetric; that is, the phenomenon of depolarization appeared. Of course, the power of the seed beam transmitted through the polarizer was equal to the power reflected within the measurement error.

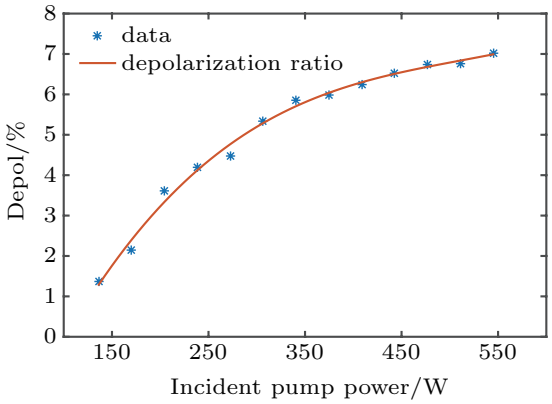


Fig. 8. Curve of the degree of depolarization as a function of pump power.

To indicate the degree of depolarization for the amplified beam, the analysis can be summarized by the following equation:

$$\text{depol} = \frac{P_{\text{B}}}{P_{\text{D}}}, \tag{18}$$

$$P_{\text{B}} = \left| P_{\text{S}} - \frac{P_{\text{S}} + P_{\text{P}}}{2} \right|. \tag{19}$$

Plugging Eq. (19) into Eq. (18),

$$\text{depol} = \frac{1}{2} \frac{|P_{\text{S}} - P_{\text{P}}|}{P_{\text{D}}} * 100\%, \tag{20}$$

where P_{S} is the power reflected by the polarizer, P_{P} is the power transmitted through the polarizer, P_{B} is the amount of deviation between reflected power and average power, and $P_{\text{D}} = P_{\text{S}} + P_{\text{P}}$ is the total power.

Bringing each value at maximum pump power into Eq. (20), the degree of depolarization of the azimuthally polarized seed beam and amplified beam can be calculated to be 1.56%, and 7.1%, respectively. To eliminate the influence of seed beam purity on the polarization degree of the amplified beam, we introduce the relative degree of depolarization to describe the change in polarization state of the amplified beam:

$$\text{depol}_{\text{r}} = \frac{\text{depol} - \text{depol}_{\text{s}}}{1 - \text{depol}_{\text{s}}}, \tag{21}$$

where depol_{r} indicates the relative depolarization of an azimuthally polarized beam, and depol_{s} indicates the degree of depolarization of the seed beam.

Finally, the relative depolarization of the azimuthally polarized light is 5.63%. This change of polarization state indicated that azimuthally polarized light had undergone depolarization after passing through a laser crystal with uneven heat distribution.

Figure 9 shows the experimental results of the beam quality factor M^2, which was measured by a commercial M^2 measuring instrument (Ophir, M^2-200 s). As shown in Fig. 9(b), the seed beam of azimuthally polarized laser exhibits $M_x^2 = 2.58$ and $M_y^2 = 2.58$ in the vertical and horizontal directions. The theoretical value of M^2 for an azimuthally polarized beam is 2 because the fundamental doughnut beam is the Laguerre–Gaussian, LG01* mode.[16] The difference between the experimental and theoretical results may be due to the master laser, which exhibited $M^2 = 1.3$ (Fig. 9(a)). The amplified beam exhibits $M_x^2 = 3.67$ and $M_y^2 = 3.71$ (Fig. 9(c)), which based on the seed beam quality factor of 2.58. We believe that the change in beam quality factor of 1.11 was caused by optical distortion during the amplification process.

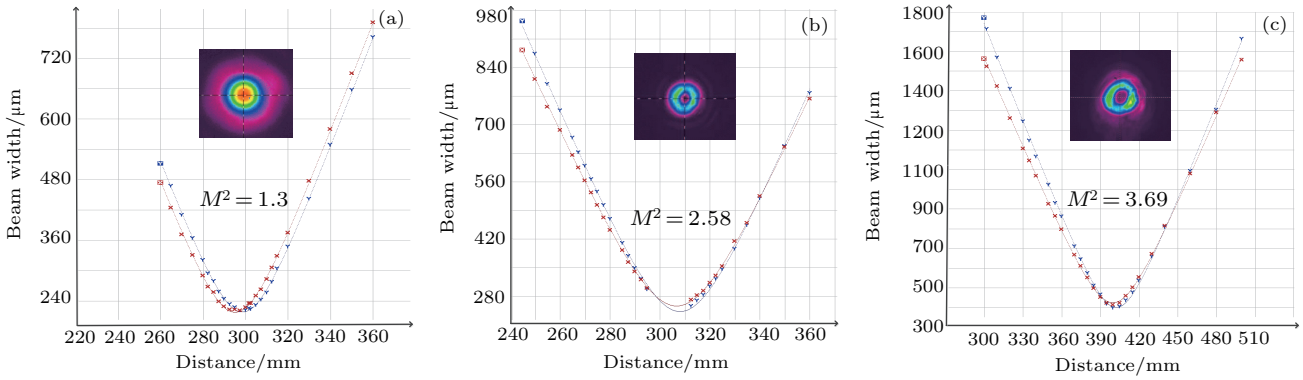


Fig. 9. Beam quality factor M^2. (a) Linear beam quality in the main laser, (b) beam quality of the azimuthally polarized seed beam, (c) amplified output beam quality.

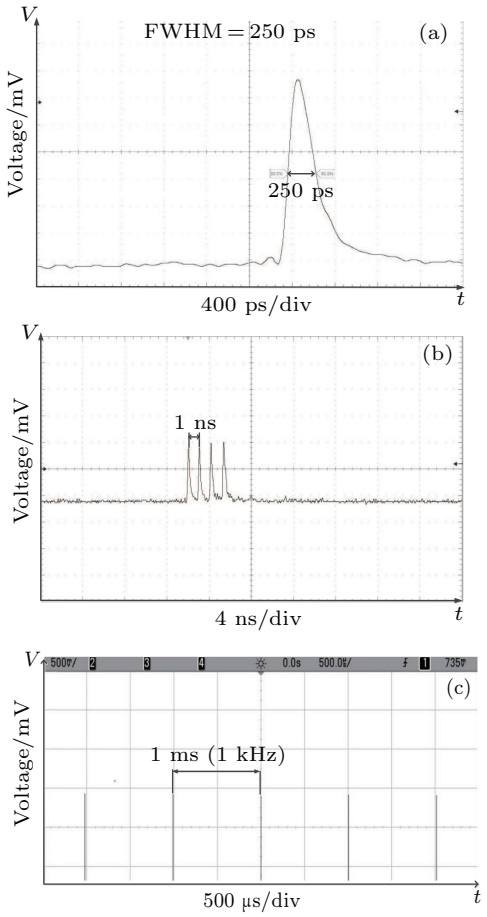


Fig. 10. Panel (a) is the pulse width of amplified output beam, panel (b) is the pulse-burst of waveform amplified output beam (four pulses separated by about 1 ns). (c) The pulse-burst repetition frequency waveform of amplified output beam.

The waveforms of amplified output beam were measured to confirm that it is pulse-burst picosecond laser. As shown in Fig. 10(a), the pulse width of the amplified beam was measured to be 250 ps. Figure 10(b) shows that there is a pulse burst, that consisted of four pulses, which have equal amplitude and a pulse spacing of 1 ns. The pulse-burst repetition frequency was 1 kHz, as shown in Fig. 10(c). The wave shape was received by a photoelectric tube with a digital phosphor oscilloscope (Tek-tronix, DPO 70604C).

4. Conclusion

In summary, an Nd:YAG amplifier and thermally induced birefringence effect for a picosecond azimuthal polarization laser were investigated. The maximum output power of the azimuthally polarized beam was 16.32 W, while the corresponding power amplification factor was 299.5%. In this work, the basic parameters of the amplified output beam were measured and the cause of the depolarization was explained. A simple criterion was defined to help estimate the amount of depolarization in an Nd:YAG amplifier system, and the relative degree of depolarization of the beam was 5.63%.

An azimuthally polarized laser with higher purity and higher power can be obtained if the uneven thermal effect of the Nd:YAG crystal is further reduced or the number of power amplifiers is increased. The generation of a high-energy pulse burst ultra-short azimuthal polarization laser is beneficial and

provides a new source reference to this development, such as material processing and welding.

References

[1] Meier M, Romano V and Feurer T 2007 *Appl. Phys. A* **86** 329
[2] Weber R, Michalowski A, *et al.* 2011 *Phys. Proc.* **12** 21
[3] Chang C, Chen X and Pu J 2017 *Opt. Rev.* **24** 188
[4] Martynas B, Mindaugas G, Peter G K and G 2011 *Appl. Phys. Lett.* **98** 201101
[5] Machavariani G, Lumer Y, Moshe I, Meir A and Jackel S 2008 *Appl. Opt.* **46** 3304
[6] Moshe I and Jackel S 2005 *J. Opt. Soc. Am. B* **22** 1228
[7] Bourderionnet J, Brignon A, Huignard J P and Frey R 2002 *Opt. Commun.* **204** 299
[8] Beresna M, Gecevicius M, Kazansky P and Gertus T 2011 *Appl. Phys. Lett.* **98** 233901
[9] Machavariani G, Lumer Y, Moshe I, Meir A and Jackel S 2008 *Opt. Commun.* **281** 732
[10] Lin D, Daniel J M O, Gecevičius M, Beresna M, Kazansky P G and Clarkson W A 2014 *Opt. Lett.* **39** 5359
[11] Kampfe T, Tonchev S, Tishchenko A V, Gergov D and Parriaux O 2012 *Opt. Express* **20** 5392
[12] Xia K G, Ueda K I and Li J L 2012 *Appl. Phys. B* **107** 47
[13] Long M L, Chen M and Li G 2017 *Chin. Opt. Lett.* **15** 49
[14] Meir A, Machavariani G, Moshe I, Jackel S and Lumer Y 2008 *Appl. Opt.* **47** 3886
[15] Koechner W andRice D 1970 *IEEE J. Quantum Electron.* **6** 557-566
[16] Loescher A, Negel J P, Graf T and Ahmed M A 2012 *Opt. Lett.* **40** 5758